NASA Technical Paper 2620

July 1986

Numerical Modeling of Physical Vapor Transport in a Vertical Cylindrical Ampoule, With and Without Gravity

Timothy L. Miller

NASA

NASA Technical Paper 2620

1986

Numerical Modeling of Physical Vapor Transport in a Vertical Cylindrical Ampoule, With and Without Gravity

Timothy L. Miller

George C. Marshall Space Flight Center
Marshall Space Flight Center, Alabama

National Aeronautics
and Space Administration

**Scientific and Technical
Information Branch**

TABLE OF CONTENTS

LIST OF ILLUSTRATIONS

TECHNICAL PAPER

NUMERICAL MODELING OF PHYSICAL VAPOR TRANSPORT IN A VERTICAL CYLINDRICAL AMPOULE, WITH AND WITHOUT GRAVITY

I. INTRODUCTION

As pointed out in some of the referenced works [1,2] the understanding of the fluid dynamics of physical vapor transport in a closed cylindrical ampoule is a fundamental requirement in understanding (and thereby possibly controlling) the crystal growth process. The prototypical system which is studied here and in previous works is shown in Figure 1. One end of the ampoule is coated with source material (A) and is at a higher temperature than that of the other end (which is initially coated with a seed material), resulting in a flow of material from the hot end to the cold end due to the difference in saturation vapor pressures. There is a "neutral" (or "buffer") gas (B) in the ampoule, the presence of which influences the fluid dynamics of the system. It is assumed that the temperatures of the endwalls are constant, and that there is no deposition upon the sidewalls of the ampoule. In the present study, the sidewalls are abiabatic (no heat flux) for some of the calculations and the sidewalls have a fixed temperature profile for others. While this system is idealized in many ways, the study of it can give rise to a fundamental understanding which can then be applied to more complicated situations (such as non-uniform endwall temperature conditions, deposition of material on sidewalls, more complex geometry, and other deviations from the prototype system).

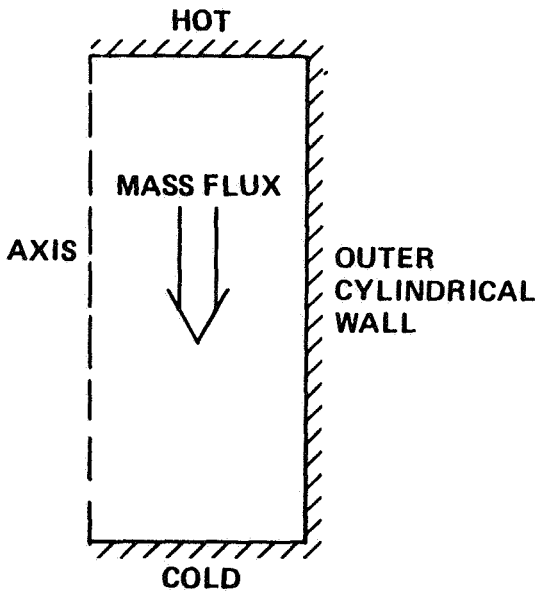

Figure 1. Schematic diagram of the prototypical crystal growth situation. Contained in the cylindrical ampoule is a gaseous mixture of components A (the growth substance) and B (a buffer gas). The gravity vector is vertical in the diagram, with direction (up or down) depending upon the case considered.

The works by Markham et al. [2] and Greenwell et al. [1] were similar to the present study in that they are numerical studies of the prototype system of Figure 1. They are based upon the same system of equations, except that the present study assumes incompressibility (i.e., the Boussinesq system of equations is used). Those previous works pointed out much of the fundamental characteristics of the fluid dynamical system, such as the important effects of the fluid's viscosity, the ampoule's aspect ratio (for fixed Peclet number, defined in the next section), buoyant convection, and the buffer gas. However, a very limited range of parameter space was studied. Furthermore, the results of independently varying the parameters were not studied in much detail. For example, showing the effect of varying aspect ratio while fixing the Peclet number gave the result that for shorter (in the axial direction) ampoules, the influence of the sidewalls was greater. However, while varying the aspect ratio, the Reynolds number was also varied (shorter ampoules had larger Reynolds number). The extent to which the result depended upon Reynolds number, rather than aspect ratio, is not clear. Other points that the present work attempts to clarify through the systematic variation of the physical parameters are: (1) the effects of the "Stefan wind" upon the onset of buoyant convection, (2) the effects of both the Stefan wind and buoyant convection upon the flux of material upon the interface, (3) the effects of different kinds of sidewall boundary conditions on temperature when buoyancy effects due to temperature variation are considered, and (4) the effects of buoyant convection due to the effects of both temperature and solute. The motivation for the present work is to offer an understanding of the fluid dynamics that may aid in explaining the differences seen in the results of ground-based and space-based experiments, especially those in a joint endeavor of NASA and the 3M Company, in which the author is a co-investigator.

II. EQUATIONS AND SOLUTION TECHNIQUE

In this study, axisymmetry is assumed. This is discussed in Markham et al. [2], and it is justifiable in cases where the buoyant convection is not too large relative to the axisymmetric gradients of temperature and solute that are forced by the Stefan flow. The savings in terms of computer and programming resources when compared with a fully three-dimensional model are, of course, considerable. It is assumed that the volume of the ampoule does not change – i.e., that the changes in the size of layers of growth and source material are very small when compared with the total volume of the ampoule. The equations used are those which describe the conservation of momentum, heat, total mass, and component A mass in a steady state:

$$0 = - V \cdot \nabla v - \frac{1}{\rho_0} \frac{\partial P}{\partial r} + \nu \left(\nabla^2 v - \frac{v}{r^2} \right) \tag{1}$$

$$0 = - V \cdot \nabla w - \frac{1}{\rho_0} \frac{\partial P}{\partial z} + \nu \nabla^2 w - g (\rho - \rho_0) \tag{2}$$

$$0 = - V \cdot \nabla T + \kappa \nabla^2 T \tag{3}$$

$$0 = - V \cdot \nabla \chi + D_{AB} \nabla^2 \chi \tag{4}$$

$$\rho = \rho_0 [1 - \alpha(T - T_0) + \beta(\chi - \chi_0)] \tag{5}$$

where the symbols are defined in Table 1. Note that variations in density due to the presence of both solute and temperature variations are included, but these variations influence the flow only through the buoyancy term. For quantitative modeling of a physical vapor transport process where large relative total density gradients are present, this assumption should not be made. For example, if the total density of the gaseous mixture is much larger at one end of the ampoule than the other, the axial velocity at that end would have to be smaller in order to conserve mass. (See the results of Greenwell et al. for the case when the molecular weights of the two materials are very different.) However, for the purpose of pointing out the fundamental behavior of the system with parameter changes, this assumption is certainly no worse for many cases than the assumptions about the ideal boundary conditions. The present calculations may be regarded as quantitatively valid for cases in which the total change in fluid density does not change by more than about 20 percent.

TABLE 1. LIST OF SYMBOLS

a	Radius of ampoule.
D_{AB}	Diffusivity of components A and B in the mixture.
g	Gravitational acceleration.
L	Axial length of ampoule.
r	Radial coordinate.
z	Axial coordinate.
P	Pressure.
T	Temperature.
T_0	Reference temperature.
T_O	Temperature at z = 0.
T_L	Temperature at z = L.
v, w	Radial and axial velocity components, respectively.
V	Velocity vector.
W	One-dimensional solution for axial velocity.
α	Thermal expansivity (density factor).
β	Solutal density factor.
ρ	Fluid density.
ρ_0	Reference density.
κ	Thermal diffusivity.
ν	Kinematic viscosity.
χ	Fractional weight concentration of component A.
ψ	Stream function.
ζ	Vorticity.

The boundary conditions on temperature have already been mentioned; fixed constant temperatures are assumed on each of the endwalls, and the sidewalls have either no-flux conditions or fixed temperature profile conditions, as identified in the description of the results. The boundary conditions on component A are of fixed, constant values at each of the endwalls and no flux through the sidewalls. No-slip conditions on the boundaries are assumed for the tangential velocity component. Impervious sidewalls are assumed, and the endwalls have the boundary condition on the axial velocity component as described in Rosenberger [3]:

$$w = \frac{-D_{AB}}{(1 - \chi)} \frac{\partial \chi}{\partial z} \quad . \tag{6}$$

This boundary condition reflects the conservation of mass as the endwalls are respectively evaporating and depositing mass of component A. It is the axial flow induced by these boundary conditions that result in the interesting aspects of the system under consideration.

There exists a well-known one-dimensional solution to the equations. If no variations in the radial direction are allowed (and the sidewalls are ignored) the axial velocity, temperature, and solute profiles are:

$$W = \frac{D_{AB}}{L} \log\left(\frac{1 - \chi_L}{1 - \chi_0}\right) \quad , \tag{7}$$

$$T(z) = \frac{(T_L - T_0)}{\exp\left(\frac{WL}{\kappa}\right) - 1} \left[\exp\left(\frac{Wz}{\kappa}\right) - 1\right] + T_0 \quad , \tag{8}$$

$$\chi(z) = \frac{(\chi_L - \chi_0)}{\exp\left(\frac{WL}{D_{AB}}\right) - 1} \left[\exp\left(\frac{Wz}{D_{AB}}\right) - 1\right] + \chi_0 \quad . \tag{9}$$

This velocity magnitude is used as the velocity scale in defining the dimensionless parameters:

$Re = aW/\nu$,	Reynolds number
$Pe = LW/D_{AB}$,	solutal Peclet number
$Pe_t = LW/\kappa$,	thermal Peclet number
$Sc = \nu/D_{AB}$,	Schmidt number
$Pr = \nu/\kappa$,	Prandtl number

$\gamma = L/a$, aspect ratio

$Ra_s = g\beta \nabla \chi a^4/\nu\kappa L$ solutal Rayleigh number

$Ra_t = g\alpha \nabla T a^4/\nu\kappa L$ thermal Rayleigh number

where only six of these parameters are independent. (Following the convention of the referenced works, the Reynolds and thermal Peclet number shall be taken to be the dependent parameters, unless stated otherwise.) For the sake of brevity, the dimensionless equations (which show where the dimensionless parameters enter the system of equations as coefficients) are not included here.

In the solution method, the momentum equations are converted to the vorticity-stream function formulation and the equations are finite differenced on a grid that is regular in the radial direction and stretched in the axial direction, with finer resolution generally placed near the cold end of the ampoule and with increased stretching for larger Pe. Partial time derivatives are included on the left hand side of the equations for vorticity, temperature, and solute, and with initial conditions of the one-dimensional analytical profiles the system is marched forward in "time" until a steady state is reached. The elliptic equation:

$$r \frac{\partial^2 \psi}{\partial z^2} + \frac{\partial}{\partial r} r \frac{\partial \psi}{\partial r} = -\zeta \quad , \tag{10}$$

is inverted at each time step by the successive line over-relaxation method to find the stream function field after the vorticity field is predicted. (A version of the model exists where the elliptic equation is solved by a direct method. This version has been used for comparison purposes. For low-resolution cases – 15 grid points in radial direction – the SLOR method is much more efficient. For high-resolution cases the direct solver can become more efficient. This is apparently due to the discontinuous boundary conditions on axial velocity component where the axial and radial boundaries meet.) From the stream function field, the boundary values of vorticity are calculated, and the velocity components are computed so that they may be used in the advective terms in the prediction equations for the next time step. Centered differencing is used in space, and the alternating-direction-implicit method is used in the diffusion terms. (In the case of vorticity, the boundary condition must be extrapolated from adjacent points in the ADI formula. This is actually done on the change in vorticity, so that for a steady-state solution this is exact within the finite difference context.) Because only a steady solution is desired, the time steps can be different for the variables with highly different diffusion parameters in order to enhance the rate of convergence. (It was found that the momentum and solute time steps must be the same, because of the coupling of the endwall boundary condition.)

Note that mass conservation requires the radially integrated axial velocity to be equal on both ends of the ampoule. The boundary condition (6) relates this velocity component to the axial gradient of component A, upon which no integral constraint can be placed without over-specifying the system. (This problem does not arise in the full, compressible system of equations, where there can be a net flux into the ampoule at a given time.) The problem was resolved by uniformly adjusting the stream function values on the endwalls at each time step, previous to the solution of the elliptic equation for the interior stream function field, so that each of the total fluxes are equal to the average of those fluxes predicted by the boundary condition (6). One of the necessary criteria used in judging a solution steady was that this adjustment asymptotically approached zero. Experience showed that this always occurred, although for some highly convective cases the time step had to be reduced for convergence to be obtained.

III. RESULTS

A. Zero-Gravity Cases

The work by Greenwell et al. [1] showed many aspects of the flow to be expected when the gravitational acceleration is zero. In that work, (1) aspect ratio was varied for fixed Peclet and Schmidt numbers when the partial pressures of components A and B were of similar magnitude – i.e., for a moderate Peclet number case (0.94), and (2) the case when the partial pressure of B is much smaller than that of A (i.e., Peclet number ~10) was studied for two aspect ratios. That study emphasized that significant deviations from the one-dimensional model results can be obtained; in particular, the radial profile of deposition upon the growth interface can become non-uniform due to the viscous effects of the sidewalls upon the flow. Note that in the Boussinesq model (the current work), temperature is a passive component in the system when gravity is zero and that the sidewall boundary condition upon temperature has no effect upon the flow and mass flux.

The first result presented here is the effect of Peclet number (and Reynolds number, since it varies along with Pe) upon the mass flux profile on the crystal interface. Figure 2 shows normalized flux versus radius for several Peclet numbers, for aspect ratio of one and Sc and Pr both = 1. As noted by Greenwell et al. [1], the flux varies radially such that the maximum flux is in the center. For the case of largest Pe (5.29) shown on that figure, the deviation from the one-dimensional value was a maximum of about 20 percent. The effect is monotonic, with increasing radial variation as the Peclet number increases. There is very little effect upon the radially integrated mass flux.

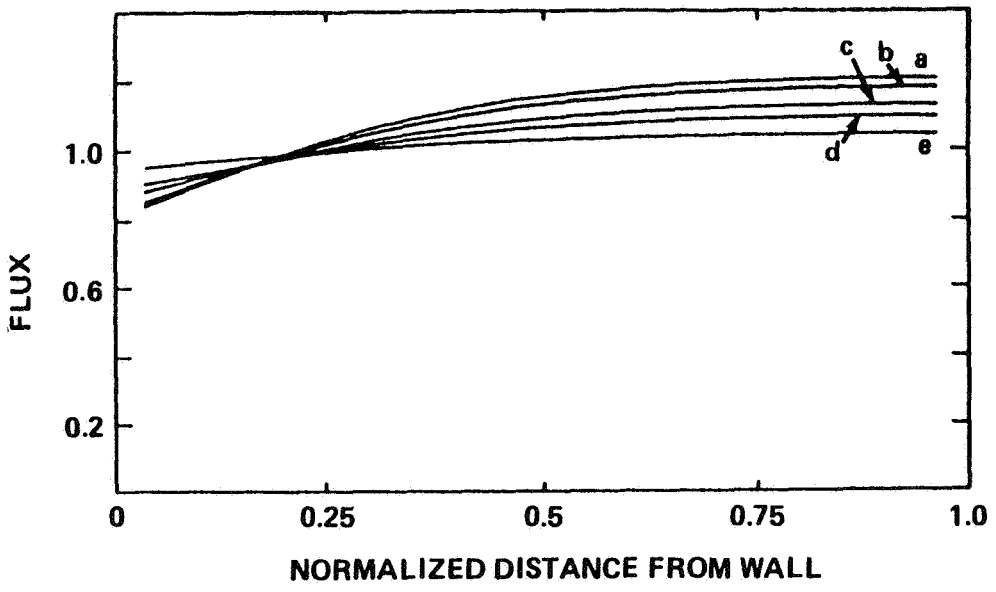

Figure 2. Normalized mass flux on the crystal interface as a function of radial distance from the sidewall for varying Pe and for fixed $\gamma = 1$, Sc = 1, and Pr = 1, and for no gravity. (a) Pe = 5.29, (b) Pe = 4.37, (c) Pe = 2.74, (d) Pe = 2.20, (e) Pe = 0.94.

The effect of aspect ratio for fixed Peclet and Reynolds number was investigated. As previously mentioned, Greenwell et al. performed this calculation for fixed Schmidt number rather than for fixed Re, and hence when the aspect ratio was smaller the Reynolds number was proportionately larger. It was not clear, then, whether increasing the axial length of the ampoule would cause a decreased effect upon the flux profile if the viscosity were also proportionately decreased so that Reynolds number were fixed. Therefore, calculations were performed in this study for Pe, Re, and Pr all = 1, for aspect ratios of 2 and 10. (Sc was 1 and 0.2, respectively, for those two cases.) Although it was hypothesized that a different result might be obtained when Re is fixed, it was found that there was more radial variation in the mass flux for the case of $\gamma = 2$. The mass flux at the center of the growth interface was 1.047 for $\gamma = 2$, and 1.016 for $\gamma = 10$. This calculation validates the conclusions of Greenwell et al., that this influence is due to aspect ratio alone, although their physical explanation should be somewhat revised. In the present, Boussinesq system – and when there is no gravity – the dimensional size of the ampoule has no effect upon the flux profile. (The length scale comes into the equations only through the Rayleigh numbers, which are zero here.) Thus, aspect ratio can be equivalently decreased by either shortening the axial length or widening the ampoule. In the latter case, contrary to Greenwell et al., there is no increase in the dimensional axial velocity. That is, the diffusive equalization of the wall-induced radial concentration gradients becomes less effective, but not because of the higher axial velocity. It is due simply to the effect of the geometry upon the flux profile in the ampoule. Figure 3 shows the profiles of axial velocity component for the two cases. Both have maximum fluid speed in the center of the ampoule, and in fact the case with $\gamma = 10$ actually has larger maximum speed (2.00) than the case with $\gamma = 2$ (max = 1.89). However, the case with a relatively long ampoule has more room (in the axial direction) to permit diffusion to bring the velocity back towards the 1-D value than does the case with the shorter ampoule, and the effect upon the flux profile at the interface is less. (That is, in the case of the shorter ampoule the growth interface is closer to the maximum axial velocity in the center, and therefore is more influenced by it.)

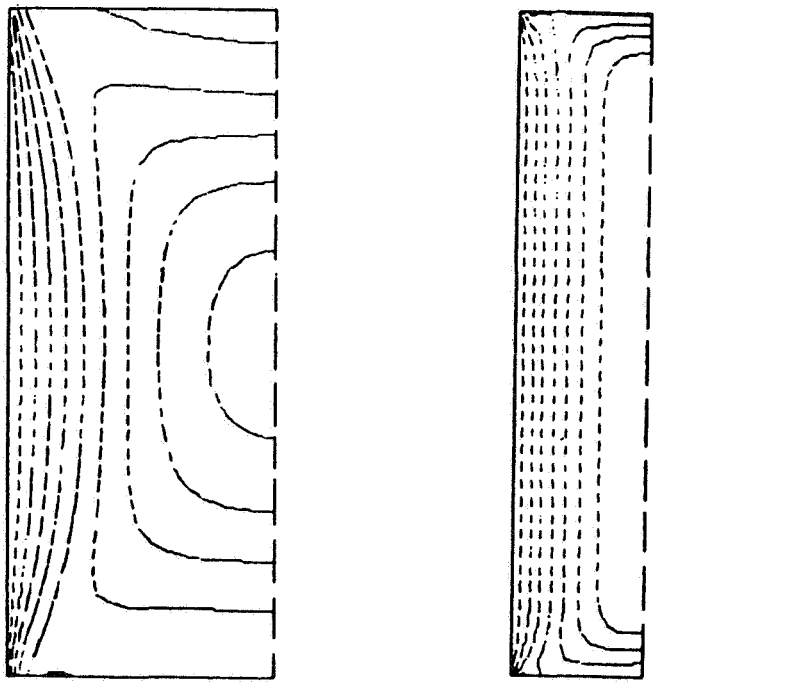

Figure 3. Contours of axial velocity (w) for aspect ratios of 2 (left) and 10 (right). The other parameters are defined in the text.

B. Single-Component Buoyant Convection

The previous work by Markham et al. [2] was of a similar model to that studied here, except that it used the compressible equations. That study considered the cases of buoyant convection due to solutal and thermal gradients separately, and investigated the effects of varying aspect ratio upon the flow. Here the variation of the dimensionless parameters Pe and Ra_t upon the flow are considered. Adiabatic sidewall boundary conditions are assumed unless indicated otherwise.

It is first noted that these calculations agree with those of Markham et al., that the "gravity-hindered" case (i.e., cold end down) is not much different from the zero-gravity case, in terms of the mass flux on the growth interface. It is possible, however, for buoyant effects to have a significant influence upon the interior flow, as discussed by Markham et al., since there exist radial gradients of temperature induced by the Stefan wind and the viscous boundary condition on the sidewall. Note that, in the adiabatic sidewall case, the effect of gravity is to inhibit circulation in the direction which would increase radial gradients. Hence, the radial gradients in the interior can be significantly reduced by the effects of the buoyancy-induced vorticity. The reader is referred to Markham et al. [2] for more details.

This report now considers the case when the ampoule is vertical, with the hot end down, and the density difference due to differing molecular weights of the materials A and B is negligible. (That is, no solutal effects on the buoyancy are considered.) Note that the parameters Pe and Ra_t are not independent in a physical crystal growing situation (larger temperature difference induces larger partial pressure difference as well as larger total density difference). However, for the purpose of elucidating the fluid dynamics of the system they shall be considered to be independent parameters – as, indeed, they are in the system of equations being used. The first question to be considered is the effect of the Stefan wind upon the transition to buoyant convection.

Figure 4 shows the normalized total diffusive heat flux across the endwalls as a function of Ra_t, for the cases Pe = 0 and Pe = 2.2. When Pe = 0, one has the classical result that the onset of convection is sudden, associated with an instability of the purely diffusive state. When there is a significant Stefan flow through the ampoule, there is no sudden onset of convection. This, of course, is due to the radial gradients in the "basic state" induced by the viscous effect of the sidewall upon the Stefan flow. These radial gradients induce buoyant convection for Ra_t smaller than the critical value for the Pe = 0 case.

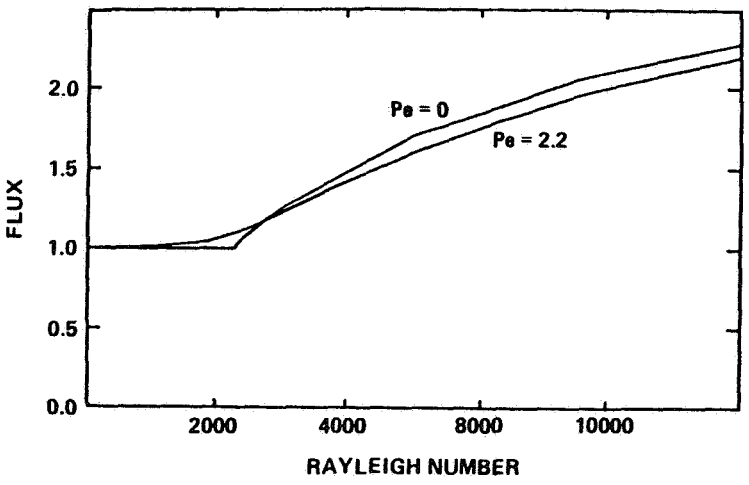

Figure 4. Nusselt number (dimensionless heat flux) as a function of thermal Rayleigh number (zero solutal Ra) for the cases of Pe = 0 (no crystal growth) and Pe = 2.2, and for aspect ratio = 1.

On the other hand, the two curves remain close to each other as Ra_t is increased, indicating that the critical Rayleigh number still has some meaning: It gives an estimate of when the buoyant effects become significant, and that the effect of the convection for a super-critical Rayleigh number does not deviate much from the classical case. For larger Pe, of course, the deviation becomes greater, although the qualitative result is not changed. Figures 5 and 6 show plots of the stream function for varying Ra_t, for the cases Pe = 0.02 and Pe = 2.2, respectively. It may be seen that the onset of buoyant convection is rather sudden for the Pe = 0.02 case, and that the strength of the buoyant convection relative to the Stefan flow builds up more gradually in the larger Stefan number case. Note that the gravity acceleration points upward in these plots. Note further that the vorticity induced by gravity in this case is in the same direction as the zero-gravity case. That is, the flow is increased in the center, and can actually be reversed in direction near the sidewall.

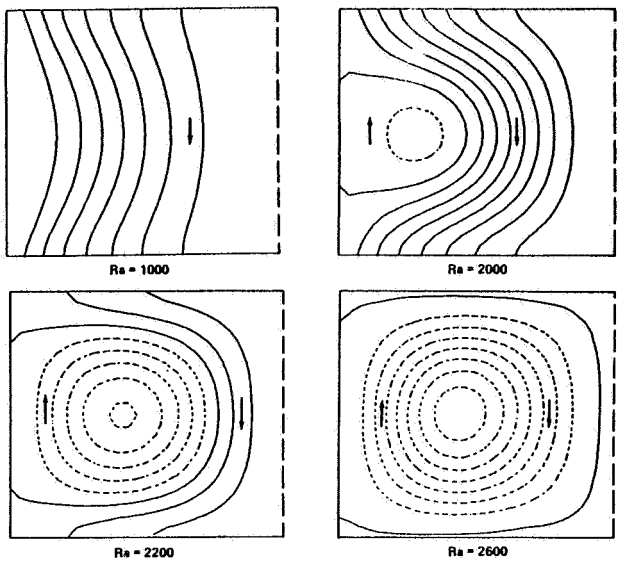

Figure 5. Stream function (the flow is parallel to the contour curves) for fixed Pe = 0.02 and varying thermal Rayleigh number. Note the rather sudden increase in the effect of buoyant convection as Ra is increased.

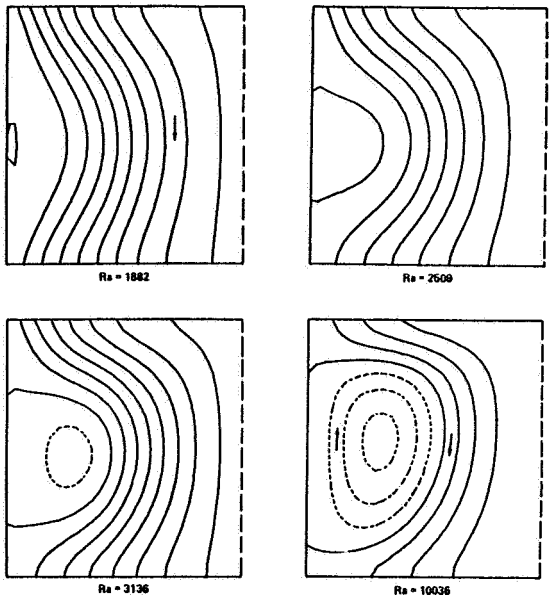

Figure 6. Stream function for fixed Pe = 2.2 and varying Rayleigh number. Note the gradual increase in the effect of buoyant convection as Ra is increased.

The effect of buoyant convection upon the mass flux at the growth interface, which was fairly mild in the cases analyzed by Markham et al., can become quite strong for sufficiently large Ra_t and fixed Pe. Figure 7 shows a plot of mass flux versus radius for Pe = 4.37 and for Ra_t ranging from about 1000 to about 4500. For the largest Ra_t case, the mass flux at the center is over twice as large as the 1-D model would predict.

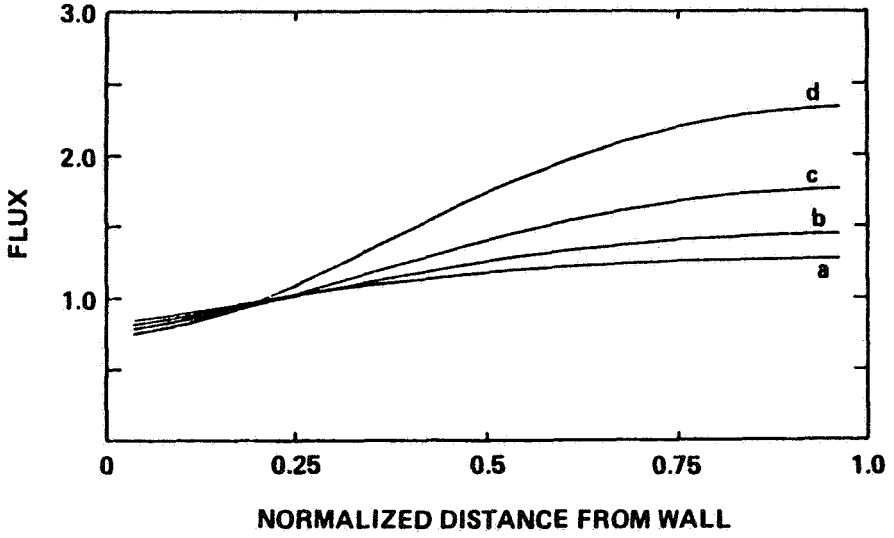

Figure 7. Normalized mass flux on the crystal interface as a function of radial distance from the sidewall for varying thermal Rayleigh number and for fixed Pe = 4.37, aspect ratio = 1, Pr = 1, Sc = 1. (a) Ra_t = 1009, (b) Ra_t = 2018, (c) Ra_t = 3027, (d) Ra_t = 4541.

The direction of the convective cell is controlled by the direction of the radial gradients in the interior of the "basic state" – i.e., the state without gravity. If the sidewall temperature is controlled to have a specific profile, the direction of these gradients can differ from those shown in the previous paragraphs. For example, the sidewall might be maintained at a rather high temperature, so that deposition on the sidewall is discouraged. In that case, most of the axial temperature gradient at the boundary is confined to a small distance near the growth interface. Diffusion tends to spread that gradient out in the interior, so that the center tends to be cooler than the region near the sidewall (at the same axial distance). Hence, the buoyant convection with the hot end down can inhibit deposition in the center, instead of encouraging it there. This effect is demonstrated in the results described below.

Some calculations were made where the sidewall boundary temperature profile was fixed at a particular profile communicated by Dr. Mark Debe, 3M Company, which is that predicted by a detailed finite-element heat transfer model (diffusion only) of the furnace that 3M has used. The conduction temperature profile in the interior is shown in Figure 8. The sidewall temperature is approximately isothermal from the hot end to a distance very close to the cold end, near which the temperature changes very quickly. There is a short distance on the endwall (0.1 of the radius) where there is a temperature gradient as well. (The boundary conditions on concentration of A remains constant on the endwall.) This particular sidewall temperature profile is one of two considered; the other profile allowed the temperature to have more variation throughout the length of the ampoule and hence did not have such strong gradients near the growth interface.

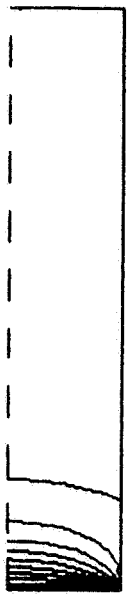

TEMPERATURE
CONTOUR INTERVAL = 0.1000

Figure 8. Contours of constant temperature for the diffusion-only field for the cases of fixed sidewall temperature profile of Figure 9.

Before discussing the computational results, it is noted that the actual physical parameters as estimated by Dr. Mark Debe of 3M result in a Rayleigh number of about only 0.14. The smallness of this number is due to the large diffusivities that were calculated. With such a small Rayleigh number, absolutely no buoyant effects are seen. Hence, the results below are for cases of diffusivities much lower than those estimated. The effects of buoyant convection can be quite different from the case with adiabatic sidewall; Figure 9 shows the results of calculation with fixed temperature profile on the sidewall. For this situation, the hot-end-down case gives rise to a reduced mass flux in the center of the growth interface, while the "gravity-inhibited" case (cold end down) results in a slight enhancement of the mass flux in the center. Since most of the radial gradients are near the growth interface, the convection is confined to that part of the ampoule. The explanation for this result is obvious. For the cold end down case, the flow must be in the direction to make the surfaces of constant density (here, isotherms) more nearly horizontal in order to attempt to minimize the potential energy. In the "unstable" case (hot end down) the flow is in the opposite direction. Generally, when hot and cold fluid is at the same height, the cold fluid will sink and the hot fluid will rise. The present results demonstrate clearly that the buoyant convection can either enhance or suppress mass deposition in the center of the growth interface, depending upon the direction of the induced circulation, which, in turn, depends upon the detail of the interior temperature profile.

C. Thermosolutal Convection

In the actual crystal-growing situation, the molecular weights of the growth substance and the buffer gas can be quite different, resulting in density gradients due to the varying concentrations of the two components. For example, the transport of organic compounds (which have large molecular weights) through argon is such a system. Here, this report shall consider the case when component A is the heavy component, resulting in the density effect due to solute being in the opposite direction as that due to heat (i.e., the effect of solute will be to make the fluid heavier at the hot end). Some actual numbers

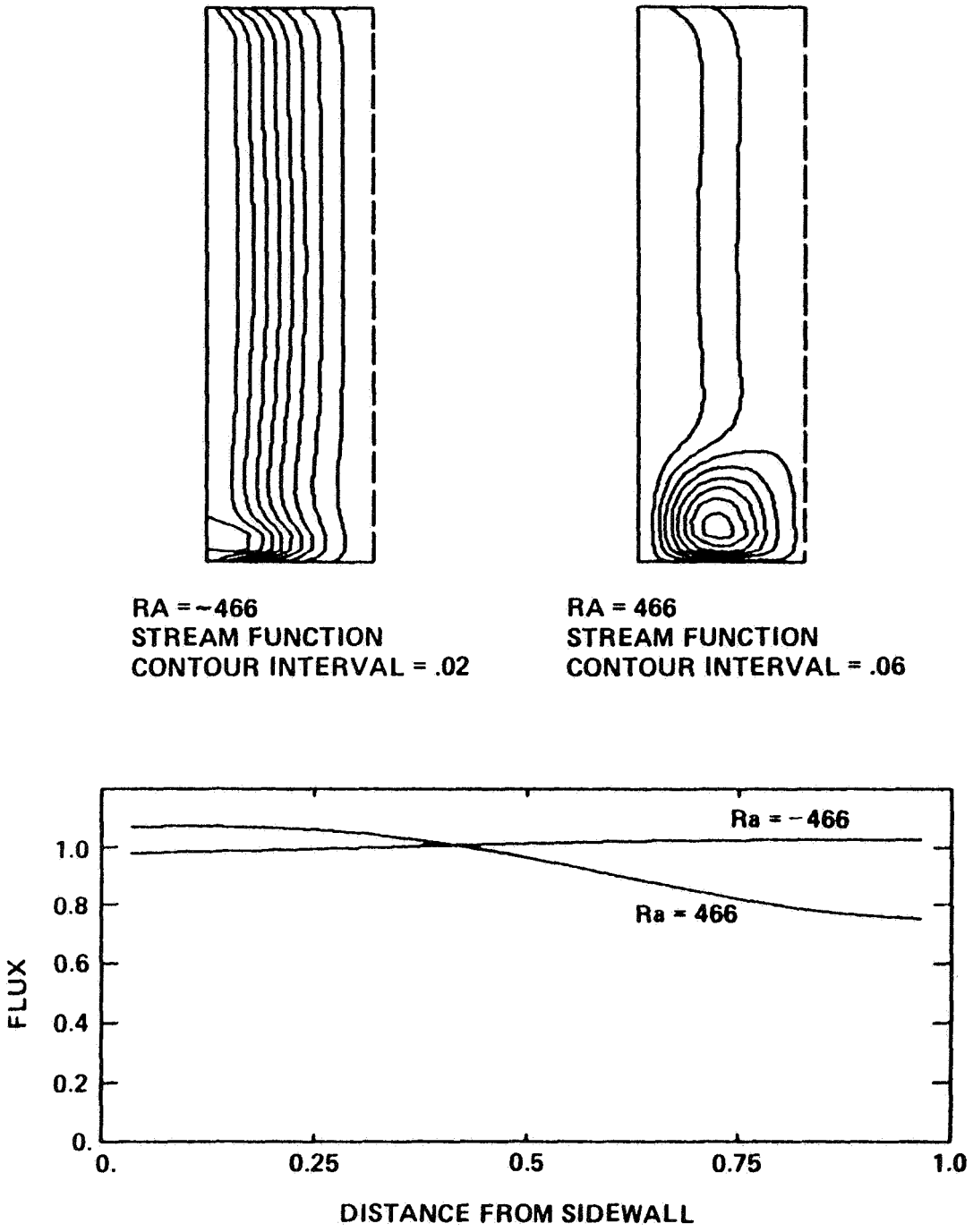

Figure 9. Stream function and mass flux for the cases of fixed sidewall temperature profile. Upper left: Stream function for the case of cold end down (Ra_t = -466). Upper right: Stream function for the case of hot end down (Ra_t = 466). Lower: Mass flux as a function of distance from the sidewall for the two cases.

for the relative concentrations of the two components in the 3M experiments have not been made available to the author; hence, calculations have been made with a broad range of solutal Rayleigh numbers for the purpose of studying the fundamental processes. Because of the very large diffusivity of solute, however, the actual Rayleigh number is probably quite small, and the cases discussed below show buoyancy effects that are much larger than those of the actual experiments.

First, it is noted that the diffusivity of solute is much larger than that of heat (by a factor of about 20), and the reader who is familiar with thermosolutal convection must reverse in his mind the role of these two components. For example, when the hot end is down, one has the "salt-finger" configuration, which here is actually "heat-finger;" the convection will be due to the more slowly-diffusing component causing convection which "ignores" the stable stratification set up by the fast-diffusing (i.e., non-conservative) component. When the cold end is down, one has the possibility of "oscillatory" convection, in which the convection is caused by the unstable gradient of the fast-diffusing component (here, solute), which eventually "breaks through" the stratification set up by the slowly-diffusing component. In this latter scenario, once the convection starts, it quickly becomes very non-linear, as the stratification set up by the more slowly-diffusing component breaks down quickly. The reader is referred to the work by Miller [4] for a further discussion of thermosolutal convection and its possible role in crystal growth.

Second, it is noted that some of the effects of solute on the buoyancy are identical to those due to heat when adiabatic sidewalls are assumed. That is, the case when the thermal Rayleigh number is small and all buoyancy effects are due to solute is essentially identical to that discussed in the previous section. Here, this report shall consider some cases where both Rayleigh numbers are large enough that there are significant buoyancy effects due to both components. Only cases with adiabatic sidewalls will be considered here.

Considering first the case with the hot end down (gravity pointing upward in the figures), Figure 10 shows the flow for a case when the total density difference due to heat is one-half that due to solute. Significant buoyant convection may be seen for this case, which has $Ra_t = 3484$. The buoyant effects may be seen despite the strong stabilizing gradient in solute for two reasons. First, the thermal gradients are mostly near the cool end of the ampoule, whereas the solutal gradients are more spread through the ampoule. This result may be thought of as a Peclet number effect; i.e., the thermal Peclet number is much larger than the solutal Pe. Second, since the diffusivity of solute is relatively large, its buoyancy effects are weak compared to that of heat. The strength of this flow is somewhat greater than that of a thermal Ra of 1742 and solutal Ra of zero.

An example of the flow for the case of cold end down is seen in Figure 11 ($Ra_s = 6969$, $Ra_t = -1742$). Here, the solutal Rayleigh number must be quite large to overcome the effect of the stabilizing thermal gradient, which inhibits convection near the growth interface. The circulation that is present is in the upper part of the ampoule. This flow is of similar magnitude to that of solutal $Ra_s = 5227$ and $Ra_t = 0$, but in the latter the circulation is closer to the growth interface and affects the flux on the growth interface somewhat more (not shown).

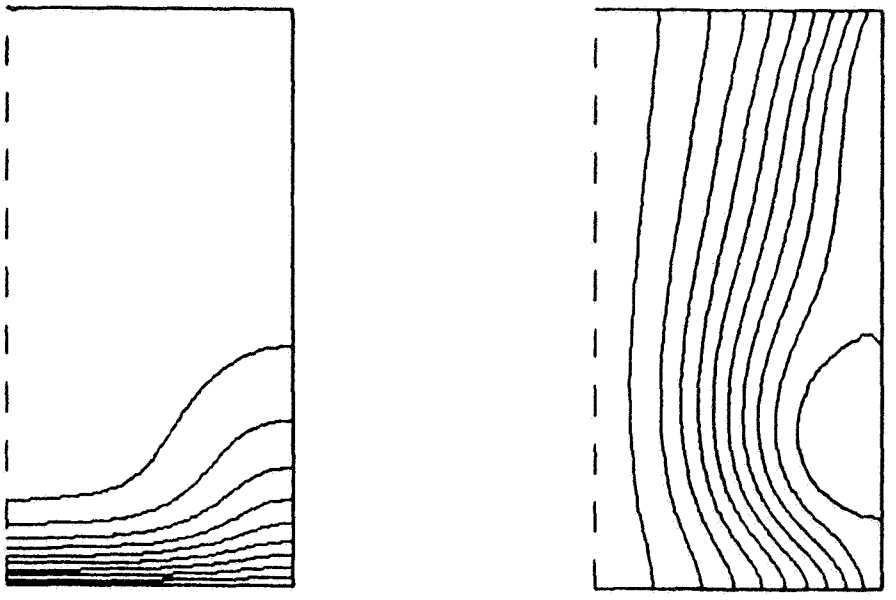

TEMPERATURE
CONTOUR INTERVAL = 0.1000

STREAM FUNCTION
CONTOUR INTERVAL = 0.2000

Figure 10. Temperature and stream function contours for the case with the hot end down and buoyancy effects of a heavy component A included as well as those due to temperature. Aspect ratio is 2, Pr = 1, Sc = 0.1, Pe = 1, Ra_t = 3484, Ra_s = -1742.

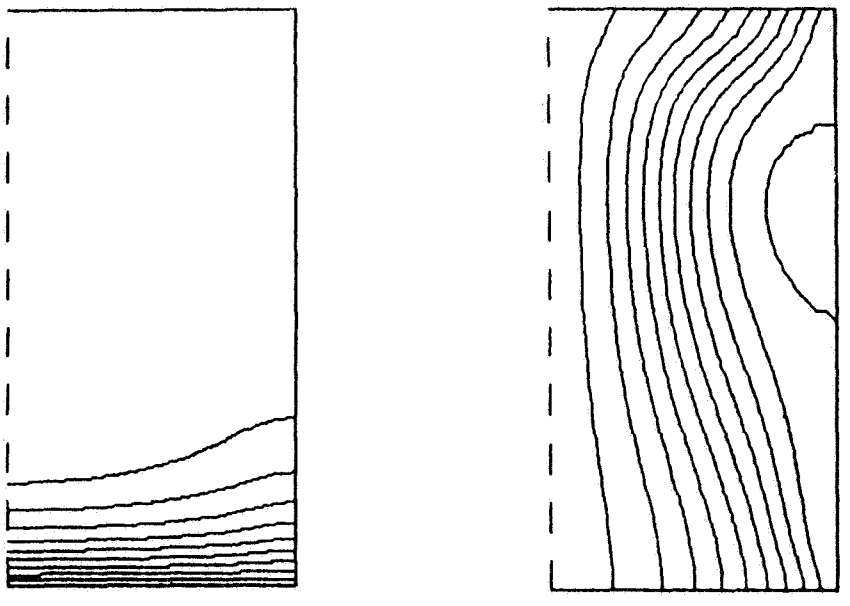

TEMPERATURE
CONTOUR INTERVAL = 0.1000

STREAM FUNCTION
CONTOUR INTERVAL = 0.2000

Figure 11. As in Figure 10, but for Ra_t = -1742 and Ra_s = 6969 (cold end down).

IV. CONCLUSIONS

The primary conclusions of the work described herein are as follows:

1) In zero-gravity convection, the radial gradients in the interior and on the growth interface increase with increasing Peclet number. For longer ampoules, this effect decreases. These results are in agreement with those of Greenwell et al. [1].

2) The effects of buoyant convection depend upon the boundary conditions on temperature (for thermally-induced buoyancy). For adiabatic sidewalls, cold end down cases are not significantly different than the zero-gravity cases. When the hot end is down, buoyant effects become significant at a Rayleigh number near the critical Rayleigh number for buoyant convection in a closed cylinder of similar aspect ratio. The direction of the buoyancy-induced circulation is such that the mass flux on the crystal interface is enhanced in the center and inhibited near the sidewall. When the temperature profile on the sidewall is fixed, the buoyant effects can become quite different, especially when the sidewall is kept warm. In that case, the direction of the buoyancy-induced circulation is such that mass deposition is inhibited in the center of the interface, and enhanced near the sidewall.

3) The effect of the Stefan wind for non-zero Peclet number is to cause a gradual transition to buoyancy-dominated flow, rather than a sudden, "critical" point, but the critical Rayleigh number remains useful as an estimate of the point at which buoyancy effects become significant.

4) When both thermal and solutal effects on the buoyancy are considered (and when the buoyancy effects are in opposite directions), the dominating effect is that due to the more slowly diffusiving component (heat). For the cold end down case, the solutal Rayleigh has to be much larger than the magnitude of the thermal Rayleigh number in order to overcome the stabilizing effect of the thermal gradient. For the hot end down case, the stable solutal gradient has a relatively small effect on the circulation induced by an unstable thermal gradient. That is, the solutal Rayleigh number can be much larger than the thermal Ra, and buoyant convection will still be present - even though the total density difference is "stable" (bottom-heavy).

REFERENCES

1. Greenwell, D. W., Markham, B. L., and Rosenberger, F.: Numerical Modeling of Diffusive Physical Vapor Transport in Cylindrical Ampoules. J. Crystal Growth, Vol. 51, 1981, pp. 413-425.

2. Markham, B. L., Greenwell, D. W., and Rosenberger, F.: Numerical Modeling of Diffusive-Convective Physical Vapor Transport in Cylindrical Vertical Ampoules. J. Crystal Growth, Vol. 51, 1981, pp. 426-437.

3. Rosenberger, F.: Fundamentals of Crystal Growth I. Macroscopic Equilibrium and Transport Concepts. Springer series in solid state science, Vol. 5, Springer-Verlag Berlin Heidelberg, New York, 530 pp, 1979.

4. Miller, T. L.: A Preliminary Study of Numerical Simulation of Thermosolutal Convection of Interest to Crystal Growth. NASA Technical Paper 2394, 33 pp, 1984.

H 1 1.60

1. REPORT NO.	2. GOVERNMENT ACCESSION NO.	3. RECIPIENT'S CATALOG NO.
NASA TP-2620		

4. TITLE AND SUBTITLE	5. REPORT DATE
Numerical Modeling of Physical Vapor Transport in a Vertical Cylindrical Ampoule, With and Without Gravity	July 1986
	6. PERFORMING ORGANIZATION CODE
7. AUTHOR(S)	8. PERFORMING ORGANIZATION REPORT #
Timothy L. Miller	
9. PERFORMING ORGANIZATION NAME AND ADDRESS	10. WORK UNIT NO.
George C. Marshall Space Flight Center Marshall Space Flight Center, Alabama 35812 N0136801	M-532
	11. CONTRACT OR GRANT NO.
	13. TYPE OF REPORT & PERIOD COVERED
12. SPONSORING AGENCY NAME AND ADDRESS	Technical Paper
National Aeronautics and Space Administration Washington, D.C. 20546	14. SPONSORING AGENCY CODE

15. SUPPLEMENTARY NOTES

Prepared by Atmospheric Sciences Division, Systems Dynamics Laboratory, Science Engineering Directorate.

16. ABSTRACT

Numerical modeling has been performed of the fluid dynamics in a prototypical physical vapor transport crystal growing situation. Cases with and without gravity have been computed. Dependence of the flows upon the dimensionless parameters aspect ratio and Peclet, Rayleigh, and Schmidt numbers is demonstrated to a greater extent than in previous works. Most notably, it is shown that the effects of thermally-induced buoyant convection upon the mass flux on the growth interface crucially depend upon the temperature boundary conditions on the sidewall (e.g., whether adiabatic or of a fixed profile, and in the latter case the results depend upon the shape of the profile assumed).

17. KEY WORDS	18. DISTRIBUTION STATEMENT
Crystal growth Physical vapor transport Fluid dynamics Numerical modeling	Unclassified-Unlimited Subject Category 27

19. SECURITY CLASSIF. (of this report)	20. SECURITY CLASSIF. (of this page)	21. NO. OF PAGES	22. PRICE
Unclassified	Unclassified	20	A02

For sale by National Technical Information Service, Springfield, Virginia 22161

NASA-Langley, 1986